Thermal Analysis and Verification of PMSM using LPTN Considering Mechanical Components and Losses

Jun-Woo Chin, Sung-Woo Hwang, Hyeon-Jin Park, and Jung-Pyo Hong, *Senior Member*, *IEEE*

***Abstract* -- In order to estimate the thermal characteristics of electric machines, the research on the lumped parameter thermal network (LPTN) has been carried out in this paper. Specifically, to improve the accuracy of the thermal analysis of the LPTN, the effect of the cooling fins on the frame, thermal modeling of bearing and the mechanical losses which can be divided into windage loss and bearing loss have been investigated. To reflect in the LPTN, the mathematical equation which describes the heat transfer through the cooling fin is derived and verified by the experiment. Moreover, the mechanical losses were obtained through experiment and divided into windage loss and bearing loss as a function of the rotational speed. Finally, the thermal analysis results ascertained through the LPTN are verified by comparing the temperature saturation test at no-load conditions. To verify the thermal analysis results, the 6-pole/9-slot interior permanent magnet synchronous machine is proposed.**

***Index Terms*-- Bearing loss, cooling fin, interior permanent magnet synchronous motor (IPMSM), iron loss, lumped parameter thermal network (LPTN), mechanical loss, windage loss.**

I. INTRODUCTION

AS the downsizing, and high power density have been required in the electric machine industry, the losses which generate the heat energy inside the machine have increased while the heat dissipation area decreases. This trend has caused the temperature of the electric machine to rise. The point is that the deterioration of the thermal characteristics can lead to the performance degradation like decrease of efficiency or the insulation failure. Therefore, the temperature prediction through the thermal analysis is significant in the design process [1], [2].

In general, the thermal analysis methods of permanent magnet synchronous motor (PMSM) can be divided into two basic types: numerical methods such as finite-element analysis (FEA) and computational fluid dynamics (CFD), and analytical lumped parameter thermal network (LPTN). The main strengths of numerical methods like FEA and CFD are the accuracy of thermal analysis and that any device geometry can be modeled [3], [4]. However, such thermal analysis using FEA and CFD takes much computational resources and time. In order to reduce such a computational resources and analysis time, the researches on hybrid thermal analysis method such as CFD coupled with LPTN are proceeding [5], [6].

Unlike FEA and CFD, the thermal analysis through the LPTN has the advantage of being very fast to calculate. For this reason, many studies on the LPTN are underway [7]-[15]. Although the thermal analysis using the LPTN is faster than the FEA or CFD, many researches are focusing on shorten the computation time of the LPTN [9], [10]. Based on the fast analysis time of the LPTN, design of the electric motor considering the thermal aspect applying the LPTN is proceeding recently [11], [12]. Also, many researchers are actively doing researches on the LPTNs for various type of electric machine [10], [11], and [13].

Even though the LPTN has been studied extensively because of its short analysis time, the LPTN has a disadvantage of less accuracy of the thermal analysis compared to FEA and CFD. The convection heat transfer coefficient, the thermal modeling of the winding and ambiguous mechanical aspects like contact state between components are the critical factors that decrease the accuracy of thermal analysis using FEA, CFD, and LPTN. As many researches on the air-gap convection [16], the thermal modeling of the stator winding [17], [18], and the critical parameters considering the mechanical aspects [19] had been progressed, the studies on improving the accuracy of the thermal analysis through LPTN are widely proceeding [14], [15].

In this regard, to improve the accuracy of the LPTN, this paper proposes the modeling and experimental verification of the LPTN considering the effect of fins on the frame, bearing and mechanical losses separated into bearing loss and windage loss. Based on the differential equation governing the heat transfer in the fin, the thermal resistance of the fin is derived and applied to the LPTN. Also, the modeling of bearing as thermal contact resistance is proposed. It has a large value so heat does not transfer well due to the point contact between the rolling element and inner or outer ring. Moreover, the mechanical loss is separated into bearing loss and windage loss empirically and reflected to their position in the LPTN respectively. Then the thermal analysis results are obtained by the proposed LPTN of interior permanent magnet synchronous motor (IPMSM). To verify the heat transfer through the fin, the experiments on the temperature gradient of fin specimens are carried out. To measure the mechanical loss, the friction torque of the proposed 6-pole/9-slot IPMSM with a non-magnetized PM is measured varying with the rotational speed. In addition, friction torque is separated into both bearing friction and windage friction, and

J. W. Chin, S. W. Hwang, H. J. Park and J. P. Hong are with the Department of Automotive Engineering, Hanyang University, Seoul 04763, Republic of Korea (e-mail: cjw1254@hanyang.ac.kr; supertramph@hanyang.ac.kr; peng1230@hanyang.ac.kr; hongjp@hanyang. ac.kr)

978-1-5386-2477-7/18/$31.00 ©2018 IEEE

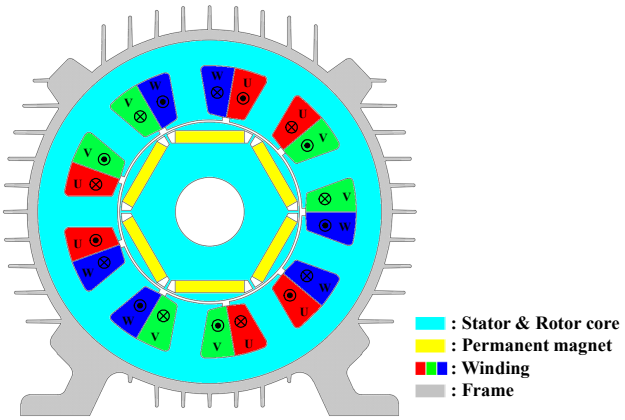

Fig. 1. Configuration of proposed IPMSM with cooling fins.

then losses are calculated by multiplying the angular velocity. Finally, the temperature saturation test of the proposed prototype IPMSM with magnetized PM is conducted at 5000rpm under no-load conditions and thermal analysis results of the proposed LPTN are compared.

II. Heat Transfer Through Cooling Fin

As shown in Fig. 1, the proposed IPMSM has cooling fins on the frame which improve heat dissipation. Fig. 2 shows the heat flow rate on a volume element and corrected fin length. Under steady conditions, the energy balance on a volume element shown in Fig. 2 (a) can be expressed as (1) [20].

$$\dot{Q}_{cond,x} = \dot{Q}_{cond,x+\Delta x} + \dot{Q}_{conv} \tag{1}$$

where, $\dot{Q}_{cond,x}$ is rate of heat conduction into the element at x, $\dot{Q}_{cond,x+\Delta x}$ is rate of heat conduction from the element at $x+\Delta x$, and $\dot{Q}_{conv}$ is rate of heat convection from the element.

Assuming a constant cross-sectional area of the fin, A_c and constant thermal conductivity, k, the differential equation governing heat transfer in the fin can be expressed as (2) by Fourier's law of heat conduction and Newton's law of cooling.

$$\frac{d^2T}{dx^2} - \frac{hp}{kA_c}(T - T_\infty) = 0 \tag{2}$$

where, x is the distance from the fin base, p is the perimeter, h is the convection heat transfer coefficient, T is the temperature of the element at x, and T_∞ is the ambient temperature.

Also the temperature gradient along the fin assuming negligible heat loss from the fin tip can be expressed as (3).

$$\frac{T(x) - T_\infty}{T_0 - T_\infty} = \frac{\cosh m(L - x)}{\cosh mL} \quad \left(\text{where, } m = \sqrt{\frac{hp}{kA_c}} \right) \tag{3}$$

An approximate, yet practical and accurate, solution to the general fin equation for considering the convection from fin tip can be derived by replacing the fin length L in the equation (3) by a corrected fin length L_c defined as (4).

$$L_c = L + \frac{A_c}{p} \tag{4}$$

The rate of heat transfer from the fin can be determined as

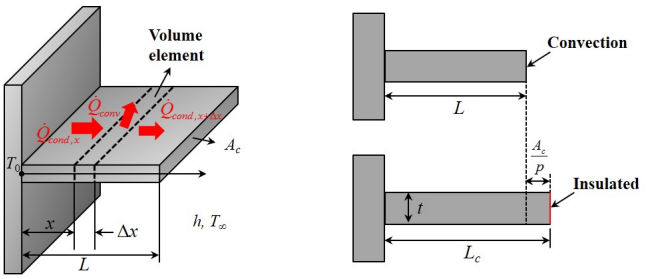

Fig. 2. Configuration of fin. (a) Heat flow rate on a volume element. (b) Corrected fin length.

(5) from Fourier's law of heat conduction and the thermal resistance can be expressed as (6).

$$\dot{Q}_{fin} = -kA_c \left.\frac{dT}{dx}\right|_{x=0} = \sqrt{hpkA_c}\,(T_0 - T_\infty)\tanh mL_c \tag{5}$$

$$R_{fin} = \frac{T_0 - T_\infty}{\dot{Q}_{fin}} = \frac{1}{\sqrt{hpkA_c}\tanh mL_c} \tag{6}$$

III. Mechanical Loss Separation

As a PM machine drives under no-load conditions, there is a no-load loss which can be separated into no-load iron loss and mechanical loss. The mechanical loss can be measured with the prototype composed by non-magnetized PM. In this paper, the experimental result of the mechanical loss is separated into bearing loss and windage loss to improve the accuracy of the thermal analysis through the proposed LPTN. Mechanical loss is composed of bearing loss and windage loss which are caused by friction torque. As expressed in (7), the friction torque from the bearing consists of the constant term and two-thirds term for the rotational speed and the friction torque from the windage consists of the quadratic term for the rotational speed respectively [21]-[25].

$$T_{friction} = T_{bearing} + T_{windage} = a_0 + a_1\omega_m^{\frac{2}{3}} + a_2\omega_m^2 \tag{7}$$

where, ω_m is the rotational speed. a_0, a_1 and a_2 are coefficients that can be obtained by least square method using experiment results.

The constant term of bearing friction torque is due to the applied load, which is empirically evaluated by Palmgren [24]. The bearing friction torque due the to applied load varies according to the magnitude and direction of the applied load, dimensions of bearing and bearing type, which are not related to the rotational speed. Additionally, the two-third term of bearing friction torque is the result of viscous friction torque, proposed by Palmgren [24]. The viscous friction torque depends on the type of bearing, the method of lubrication, the property of lubrication oil, dimensions of bearing, and the rotational speed. Specifically for the prototype proposed in this paper, the ball bearing is used.

As the rotor of PM machine rotates, there are frictions between the rotor and airgap, stator and airgap because of force due to the shear stress of the fluid [23]. From the view point of aerodynamics proposed in [23], this force produces windage friction torque depending on the quadratic term for the rotational speed. Moreover the windage friction torque depends on the radius of the rotor, axial length of the rotor,

air density, and skin friction coefficient which is the function of Reynolds number.

Accordingly, the mechanical losses can be calculated by multiplying the equation (7) by the angular velocity. For the purpose of improving the accuracy of thermal analysis through the proposed LPTN, the separated bearing loss and windage loss are reflected in proper part of PMSM in the proposed LPTN. The details are explained in chapter IV.

IV. Lumped Parameter Thermal Network

A. Background

The LPTN is organized based on the thermal network proposed by P. H. Mellor [26]. Since the shape of almost component of the rotating electric motor are cylindrical shape basically, thermal resistances and capacitances are calculated based on hollow cylinder shape. The mechanisms of heat flow through the conduction, the convection and the complex contact states between parts are modeled as resistances in electric circuit based on the assumptions below.

1) Radiation is ignored
2) No heat flows in a circumferential direction except for the flow between the stator teeth and windings
3) The thermal capacitance and the heat source are uniformly distributed in each component

After all the thermal resistances, thermal capacitances and losses compose the LPTN, it is solved based on the linear differential equation as expressed in (8) for all node.

$$C_i \frac{dT_i}{dt} = \frac{1}{R_{ji}}\left(T_j - T_i\right) + \dot{Q}_i \tag{8}$$

where C_i is the node thermal capacitance, T_i, T_j are the ith and jth node temperature, R_{ji} is thermal resistance between two adjacent nodes, i and j, and $\dot{Q}_i$ is loss at node i and it can be expressed as rate of heat generation at node i.

The conduction occurs inside each part of the electric motor such as the rotor, stator yoke, stator tooth, stator tooth tip, permanent magnet (PM) and frame. Due to the shape of the electric motor, particularly for the IPMSM, all these parts can be equivalent to a hollow cylindrical shape in (a) of Fig. 3. Each conduction component is modeled as the circuit shown in (b) of Fig. 3, applying the axial periodicity. It consists of the four thermal conduction resistances. The R_a represents the resistance in the axial direction. The R_{1r}, R_{2r}, and R_{mr} represent the resistances of the radially outward and inward direction, and compensation, respectively.

For convection in electric motors, the thermal convection resistance, $R_{convection}$ in (9) is related to not only the dimension but also the state of the air flow.

$$R_{convection} = \frac{1}{hA} \tag{9}$$

where A is the surface area where the convection occurs, and h is the convection heat transfer coefficient. The three cases of convection are considered as follow.

1) Frame - ambient
2) Air gap: stator - rotor
3) Air between end cover and stator, end cover and rotor

The convection heat transfer coefficient of above cases are decided by the empirical equations investigated beforehand [16], [20].

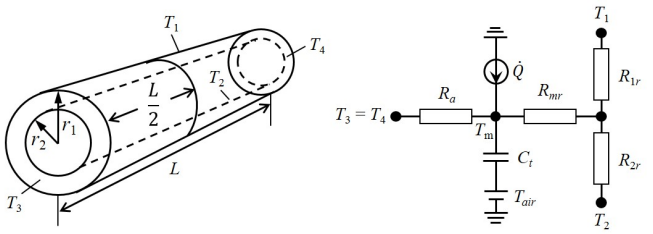

Fig. 3. General hollow cylindrical component. (a) Hollow cylindrical model. (b) Thermal network for hollow cylindrical model.

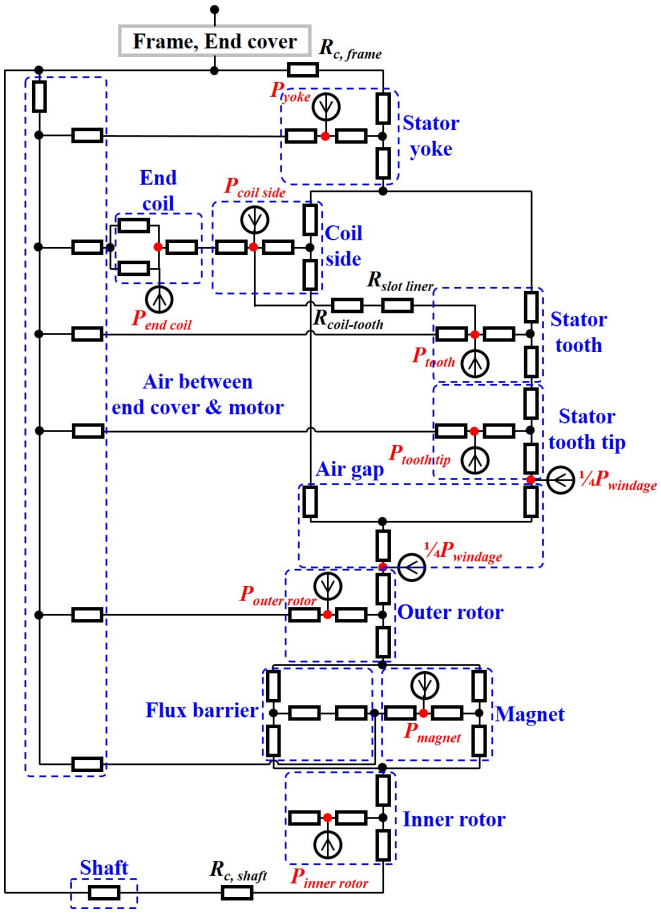

Fig. 4. Lumped parameter thermal network for the IPMSM.

The heat sources are the losses of the electric motors such as the mechanical loss, the iron loss, the copper loss, and the eddy current loss in the PM. The heat sources are expressed as the current source in the thermal network. As shown in Fig. 4, the heat sources are separated in detail so as to predict the temperature according to the exact location of the electric motor. For the copper loss, the coil is separated into the end coil and the coil side. $P_{end\ coil}$ and $P_{coil\ side}$ are the separated copper losses. For the iron loss, it is departmentalized by position of the loss generation as the stator yoke, the stator tooth, the stator tooth tip, the outer rotor, and the inner rotor. The separated iron losses, P_{yoke}, P_{tooth}, $P_{tooth\ tip}$, $P_{outer\ rotor}$, and $P_{inner\ rotor}$ are shown in Fig. 4. In this paper, the copper loss is ignored because there is no current input when driving the

proposed IPMSM under no-load condition. Also, the eddy current loss in PM is ignored because of its small value.

The thermal capacitance is calculated with dimensions, mass density, ρ and specific heat, c_p of the material by (14).

$$C = \rho c_p \pi \left(r_1^2 - r_2^2 \right) L \tag{10}$$

B. Consideration of Heat Transfer through Cooling Fins

There are many fins on the frame of the proposed IPMSM as shown in Fig. 1. According to (6) of chapter II, each fin can be expressed as the thermal resistance and connected to the outer side of the frame in parallel with the convection thermal resistance of the frame $R_{frame,\ convection}$ in Fig.5. Actually, the direction of cooling fins (straight up, straight down, horizontal) influences the heat dissipation of fins because of different air flow conditions surrounding the fins. However, it is not efficient to model all the fins as the thermal resistance and so such a method costs more in terms of computation time. Therefore, in assumption that the air flow conditions surrounding fins are the same with different directions, the average thermal resistance of the fin is proposed in this paper. By replacing the fin length L, the cross-sectional area of the fin A_c, and the perimeter p into the average fin length, average cross-sectional area, and average perimeter respectively in (4), (6), the average thermal resistance of fin $R_{fin,\ avg}$ can be obtained. Finally, the effect of heat transfer through cooling fins is considered in the proposed LPTN by connecting $R_{fin,avg}$ in parallel with $R_{frame,\ convection}$ as shown in Fig. 5.

C. Consideration of Bearing and separated Mechanical Losses

As discussed in chapter III, the purpose of mechanical loss separation is to improve the accuracy of thermal analysis through the proposed LPTN. Therefore, it is also significant to reflect the separated mechanical loss as an appropriate part of the proposed LPTN from the viewpoint of accuracy. Also, the modeling of bearing in the LPTN is important in terms of the prediction of the rotor temperature. Generated heat in the rotor transfer only through convection on the rotor surface and conduction through the shaft, bearing and end cover. However, it is very difficult to model the thermal resistance of the bearing because of its complex structure. Therefore, the modeling of bearing in the LPTN is proposed as below.

As shown in Fig. 6 (a), the bearing friction occurs between the rolling element and inner ring, as well as the rolling element and outer ring because of the applied load and viscous friction. From the viewpoint of heat transfer, heat transfer between the inner ring and the outer ring is difficult because both the inner and the outer ring are in point contact with the rolling element. Therefore, the bearing is modeled as thermal contact resistance as shown in Fig. 6 (b), which has a large value so heat is not transferred easily [24], [25]. In addition, the bearing losses are divided in half and reflected on both sides of the thermal resistance, each representing a loss between the inner ring and the rolling element, and a loss between the outer ring and the rolling element. Since the bearing is on both sides in the axial direction, the loss is divided by one-fourth as shown in Fig. 6 (b).

There are frictions from the windage between the rotor and airgap, as well as the stator and airgap as the rotor of the PM machine rotates. Since windage friction occurs on both surfaces of the rotor and stator, the windage loss is divided in half and applied to each surface of the rotor and stator in the proposed LPTN as expressed in Fig. 4.

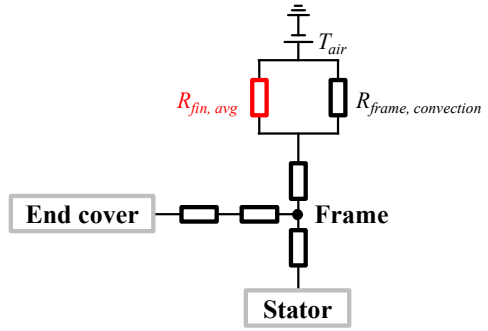

Fig. 5. Reflected position of average thermal resistance of fin in LPTN.

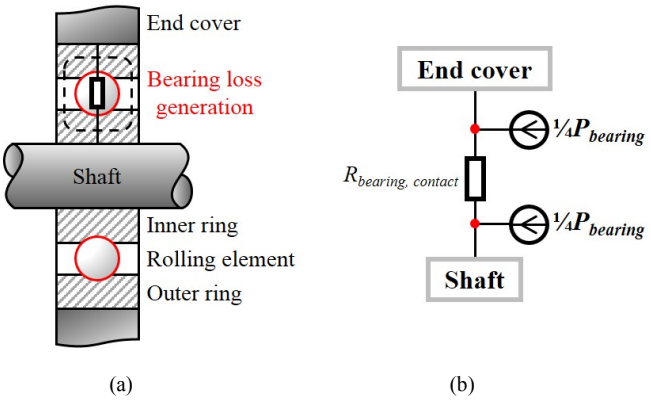

Fig. 6. Configuration of bearing. (a) Position of loss generation in bearing. (b) Reflected position of bearing loss in LPTN.

V. Verification

In this chapter, one experiment and two tests were conducted. To verify the heat transfer through the cooling fin, the experiments on the temperature gradient of cooling fins were carried out. To separate the mechanical losses into bearing loss and windage loss, the friction torque of the proposed prototype IPMSM with a non-magnetized PM was measured varying with the rotational speed. In addition, friction torque was separated into both bearing friction and windage friction, and then mechanical losses were calculated by multiplying the angular velocity. Finally, the temperature saturation test of the proposed prototype IPMSM with a magnetized PM was conducted at 5000rpm, under no-load conditions. Details about the experiment and tests are as explained below.

A. Experiment on Heat Transfer through Cooling Fin

In chapter II, the thermal resistance of the cooling fin is derived from the differential equation governing heat transfer in the fin. However, it is hard to verify the value of thermal resistance. Instead of verifying the value of thermal resistance directly, the temperature gradient along the fin (3), replacing the fin length L to corrected fin length L_c, was measured and verified through experiment. Three specimens were measured and the dimensions of the fins were listed in Table I. The

TABLE I
Dimensions of Fin Specimens

Specimen	Length(mm)	Width(mm)	Thickness(mm)
Fin A	200	30	2
Fin B	150	30	2
Fin C	200	30	4

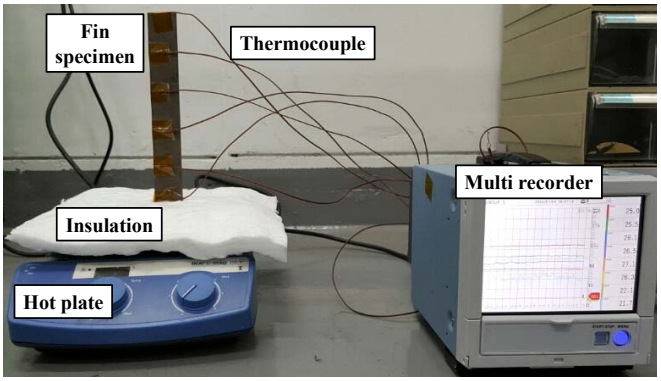

Fig. 7. Experimental set for verifying heat transfer through cooling fin

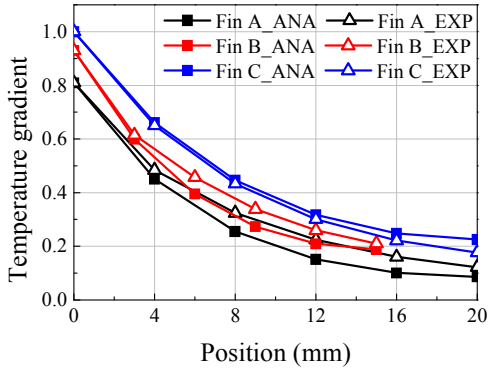

Fig. 8. Temperature gradients along fin specimens.

material of the fin was FCD450, which is the same as the frame of the prototype IPMSM. The experiments were performed by the experimental set shown in Fig.7. Six points of temperature were measured for each specimen and the results of the temperature gradient along the fin were shown in Fig. 8. The largest error between the analytic and experimental result was less than 10% and its trends are similar enough between the analytic and experimental results.

B. Measurement of Friction Torque and Mechanical Loss Separation

As previously explored in chapter III, there is a no-load loss that consists of no-load iron loss and mechanical loss when driving a PM machine under no-load condition. To measure the friction torque and calculate the mechanical loss accurately, the prototype of the PM machine with a non-magnetized PM is needed. In this paper, the prototype of the proposed IPMSM with a non-magnetized PM was manufactured and conducted the test to measure the friction torque. The dimensions are summarized in Table II. As shown in Fig. 9, the test was set by the prototype of the proposed IPMSM using non-magnetized PM when measuring the friction torque. Because of the viscosity of the lubrication

TABLE II
Dimensions for Prototype of proposed IPMSM and losses @5000rpm

Quantity	Unit	Value
Pole / slot	-	6 / 9
Outer diameter (Stator / Rotor)	mm	230
Airgap length	mm	1.5
Stack length	mm	160
Core material	-	35PN230
PM Residual induction	T	1.30
Bearing loss	W	29.4
Windage loss	W	56.9
Stator yoke iron loss	W	206.7
Stator tooth iron loss	W	142.5
Stator tooth tip iron loss	W	49.5
Outer rotor iron loss	W	15.2
Inner rotor iron loss	W	8.9

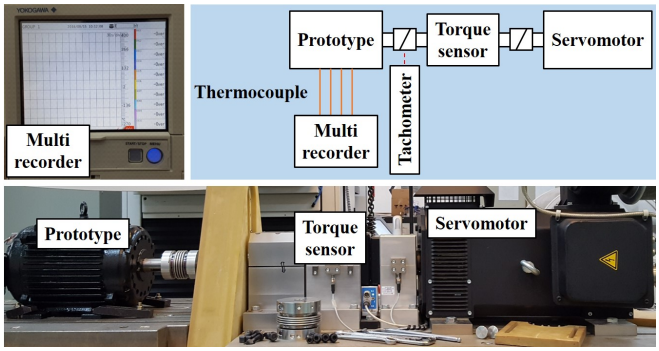

Fig. 9. Test set for measuring friction torque and temperature saturation.

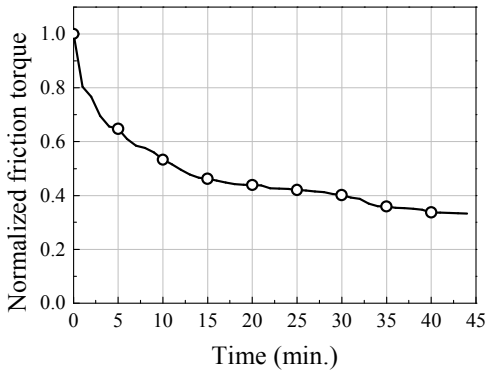

Fig. 10. Normalized friction torque according to time.

oil in the bearing, the bearing is not lubricated enough when the driving duration time remains short. It results in the friction torque to differ along the driving time. Therefore the friction torque was measured after enough time had passed as shown in Fig. 10. Then the friction torque varying with the rotational speed was measured and separated into bearing friction torque and windage friction torque as shown in Fig. 11 (a). Afterwards the mechanical losses were calculated by the friction torque as shown in Fig. 11 (b).

C. Temperature Saturation Test under No-load Condition

In the temperature saturation test, the test was set by the prototype of the proposed IPMSM using the magnetized PM

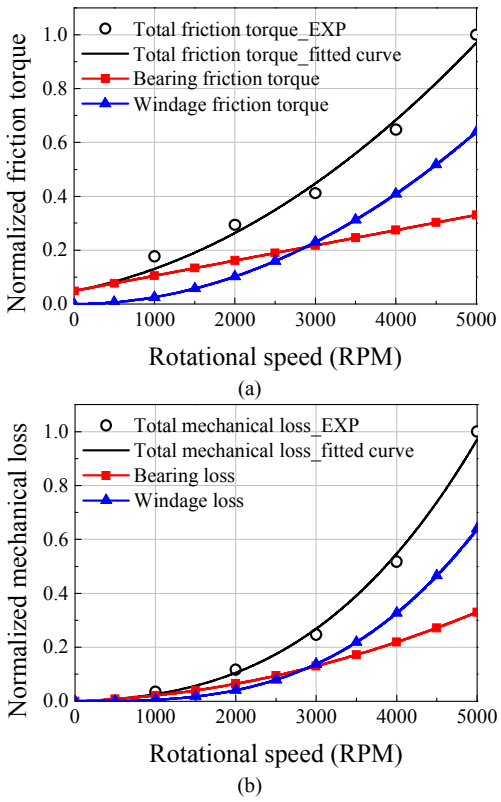

Fig. 11. Normalized friction torque and mechanical loss according to rotational speed. (a) Friction torque. (b) Mechanical loss.

as shown in Fig. 9. As the servomotor drive the prototype at 5000rpm, no-load conditions, the torque resulting in a no-load loss was measured. In addition, the rotational speed and temperature of each of the three points of the end coil, stator yoke, and housing were measured respectively. By subtracting the mechanical loss from the no-load loss, the no-load iron loss was obtained. The no-load iron loss is divided into stator yoke, stator tooth, stator tooth tip, outer rotor, and inner rotor iron loss respectively by referring the 2-D FEA result. The losses generated at 5000rpm, no-load condition are listed in Table II. Then all the separated losses are reflected as heat sources in the proposed LPTN.

To measure the rotor temperature in the temperature saturation test, the temperature of PM was estimated by the reduced fundamental of no-load back electromotive force (EMF). Right before and after the temperature saturation test, the no-load back EMF was measured at 5000rpm. The residual induction of the PM after the temperature saturation test is estimated through a proportional calculation with the analytical value. By calculating the residual induction, the temperature of PM could be estimated. The measured and analysis result for fundamental of no-load back EMF at 5000rpm was 223Vrms at room temperature 25℃. Right after the temperature saturation test, the measured fundamental of no-load back EMF at 5000rpm was 210.2Vrms. Therefore the estimated PM temperature was 93℃.

Finally, as shown in Fig. 12, the thermal analysis results from the proposed LPTN were compared with the average temperature of three points of the (a) end coil, (b) stator

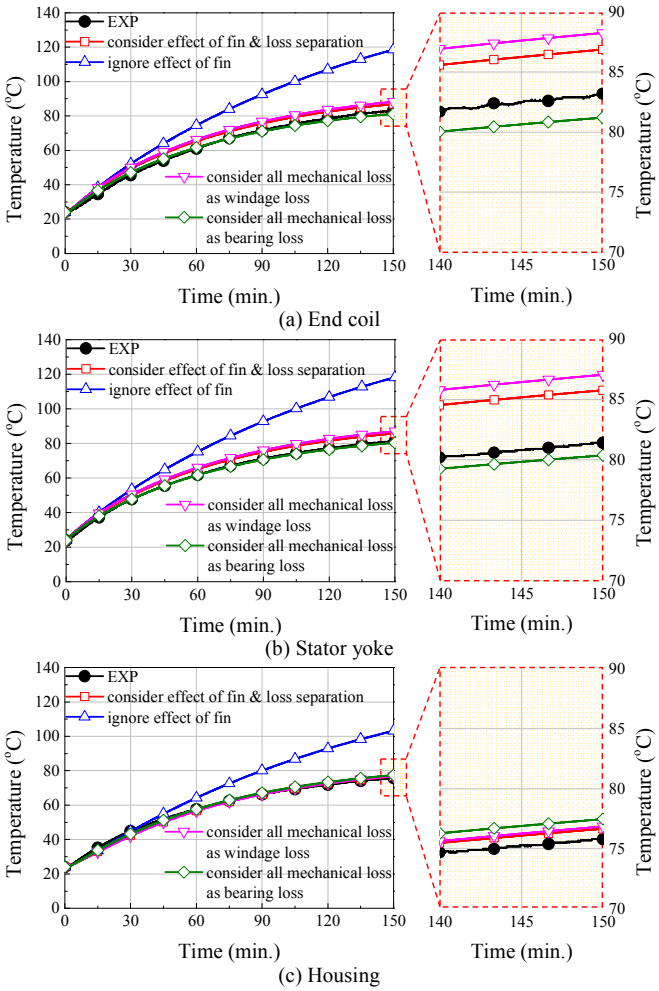

Fig. 12. Comparison of thermal analysis results and temperature saturation test results. (a) End coil. (b) Stator yoke. (c) Housing.

yoke, and (c) housing respectively. Also the temperature of the PM at 150 minute of driving time was 93.7℃ considering the effect of cooling fin and loss separation. The accuracy of the thermal analysis had improved in comparison to the thermal analysis results ignoring the effect of the fin, considering all mechanical loss as windage loss, and considering all mechanical loss as bearing loss.

VI. Conclusion

This paper proposes the modeling and verification of the LPTN considering the effect of cooling fins, bearing and mechanical loss separation. The thermal resistance of the fin is applied to the LPTN considering the heat transfer in the fin. Also, the bearing is modeled as thermal contact resistance which has a large value because of the contact state between rolling element and inner or outer ring. Moreover, the separated losses such as bearing loss and windage loss are reflected to their position in the LPTN respectively.

The experiments on the temperature gradient of fin specimens are carried out to verify the heat transfer through the fin. The friction torque of the proposed 6-pole/9-slot prototype IPMSM with a non-magnetized PM is measured varying with the rotational speed to measure the mechanical loss. The temperature saturation test of the proposed

prototype IPMSM with magnetized PM is conducted at 5000rpm under no-load conditions and thermal analysis results of the proposed LPTN are compared.

As a result, the temperature gradients of the experimental and analytical values fit well within an error of less than 10% for 3 different fin specimens. In addition, the temperature differences at 150 minute of driving time between the results through the proposed LPTN, considering the effect of cooling fin and loss separation, and test results are 4.0℃, 4.3℃, 2.0℃, and 0.7℃ for end coil, stator yoke, housing and PM, respectively. Moreover, the trend between these results are more similar than other analysis conditions. Especially for considering all mechanical loss as bearing loss, the temperatures of end coil and stator yoke are higher than the test results while that of housing is lower than the test results. Also, the temperatures of end coil and stator yoke become higher when considering all mechanical loss as windage loss while that of housing is similar. Therefore the proposed LPTN is reasonable to analyze the thermal characteristics of PMSM.

VII. REFERENCES

[1] A. Boglietti, A. Cavagnino, D. Staton, M. Shannel, M. Mueller, and C. Mejuto, "Evolution and Modern Approaches for Thermal Analysis of Electrical Machines," *IEEE Trans. Ind. Electron.,* vol. 56, no. 3, pp. 871-882, Mar. 2009.

[2] D. Staton, A. Boglietti, and A. Cavagnino, "Solving the More Difficult Aspects of Electric Motor Thermal Analysis in Small and Medium Size Industrial Induction Motors," *IEEE Trans. Energy Convers.*, vol. 20, no. 3, pp. 620-628, Sep. 2005.

[3] D. A. Howey, A. S. Holmes, and K. R. Pullen, "Measurement and CFD Prediction of Heat Transfer in Air-Cooled Disc-Type Electrical Machines," *IEEE Trans. Ind. Appl.*, vol. 47, no. 4, pp. 1716-1723, Jul/Aug. 2011.

[4] P. H. Connor, S. J. Pickering, C. Gerada, C. N. Eastwick, C. Micallef, and C. Tighe, "Computational fluid dynamics modelling of an entire synchronous generator for improved thermal management," *IET Electr. Power Appl.*, vol. 7, no. 3, pp. 231–236, 2013.

[5] J. Dong, Y. Huang, L. Jin, B. Guo, H. Lin, J. Dong, M. Cheng, and H. Yang, "Electromagnetic and Thermal Analysis of Open-Circuit Air Cooled High-Speed Permanent Magnet Machines With Gramme Ring Windings," *IEEE Trans. Magn.,* vol. 50, no. 11, pp. 1-4, Nov. 2014.

[6] Y. Wang, D. M. Ionel, and D. Staton, "Ultrafast Steady-State Multiphysics Model for PM and Synchronous Reluctance Machines," *IEEE Trans. Ind. Appl.*, vol. 51, no. 5, pp. 3639-3646, Sep/Oct. 2015.

[7] B. H. Lee, K. S. Kim, J. W. Jung, J. P. Hong, and Y. K. Kim, "Temperature Estimation of IPMSM Using Thermal Equivalent Circuit," *IEEE Trans. Magn.*, vol. 48, no. 11, pp. 2949-2952, Nov. 2012.

[8] O. Wallscheid and J. Böcker, "Global Identification of a Low-Order Lumped-Parameter Thermal Network for Permanent Magnet Synchronous Motors," *IEEE Trans. Energy Convers.*, vol. 31, no. 1, pp. 354-365, Mar. 2016.

[9] C. Sciascera, P. Giangrande, L. Papini, C. Gerada, and M. Galea, "Analytical Thermal Model for Fast Stator Winding Temperature Prediction," *IEEE Trans. Ind. Electron.,* vol. 64, no. 8, pp. 6116-6126, Aug. 2017.

[10] A. Tessarolo and C. Bruzzese, "Computationally Efficient Thermal Analysis of a Low-Speed High-Thrust Linear Electric Actuator With a Three-Dimensional Thermal Network Approach," *IEEE Trans. Ind. Electron.,* vol. 62, no. 3, pp. 1410-1420, Mar. 2015.

[11] Y. Chen, X. Zhu, L. Quan, and L. Wang, "Performance Analysis of a Double-Salient Permanent-Magnet Double-Rotor Motor Using Electromagnetic-Thermal Coupling Method," *IEEE Trans. Appl. Supercond.,* vol. 26, no. 4, Jun. 2016, Art. no. 5205305.

[12] C. López-Torres, A. Garcia, J. Riba, and L. Romeral, "Design and optimization for vehicle driving cycle of rare-earth-free SynRM based on coupled lumped thermal and magnetic networks," *IEEE Trans. Veh. Technol.,* vol. PP, no. 99, pp. 1-1, 2017.

[13] H. Li and Y. Shen, "Thermal Analysis of the Permanent-Magnet Spherical Motor," *IEEE Trans. Energy Convers.,* vol. 30, no. 3, pp. 991-998, Sep. 2015.

[14] A. Boglietti, E. Carpaneto, M. Cossale, and S. Vaschetto, "Stator-Winding Thermal Models for Short-Time Thermal Transients: Definition and Validation," *IEEE Trans. Ind. Electron.*, vol. 63, no. 5, pp. 2713-2721, May. 2016.

[15] J. Nerg, M. Rilla and J. Pyrhönen, "Thermal Analysis of Radial-Flux Electrical Machines With a High Power Density," *IEEE Trans. Ind. Electron.*, vol. 55, no. 10, pp. 3543–3554, Oct. 2008.

[16] D. A. Howey, P. R. N. Childs, and A. S. Holmes, "Air-gap convection in rotating electrical machines," *IEEE Trans. Ind. Electron.*, vol. 59, no. 3, pp. 1367–1375, Mar. 2012.

[17] F. Ahmed and N. C. Kar, "Analysis of End-Winding Thermal Effects in a Totally Enclosed Fan-Cooled Induction Motor with a Die Cast Copper Rotor," *IEEE Trans. Ind. Appl.*, vol. 53, no. 3, pp. 3098–3109, May/Jun 2017.

[18] N. Simpson, R. Wrobel, and P. H. Mellor, "Estimation of equivalent thermal parameters of impregnated electrical windings," *IEEE Trans. Ind. Appl.*, vol. 49, no. 6, pp. 2505-2515, Nov/Dec. 2013.

[19] A. Boglietti, A. Cavagnino, and D. Staton, "Determination of Critical Parameters in Electrical Machine Thermal Models," *IEEE Trans. Ind. Appl.*, vol. 44, no. 4, pp. 1150–1159, Jul/Aug. 2008.

[20] Y. A. Cengel and A. J. Ghajar, *Heat and Mass Transfer, Fundamentals and Applications, 5th ed*. McGraw-Hill Education, New York, NY, 2015.

[21] R. Wrobel, P. Mellor, M. Popescu, and D. Staton, "Power Loss Analysis in Thermal Design of Permanent Magnet Machines – A Review," *IEEE Trans. Ind. Appl.*, vol. 52, no. 2, pp. 1359–1368, Mar/Apr. 2015.

[22] R. Wrobel, G. Vainel, C. Copeland, T. Duda, D. Staton, and P. H. Mellor, "Investigation of Mechanical Loss Components and Heat Transfer in an Axial-Flux PM Machine," *IEEE Trans. Ind. Appl.*, vol. 51, no. 4, pp. 3000–3011, Jul/Aug. 2015.

[23] J. E. Vrancik, "Prediction of Windage Power Loss in Alternators," *NASA Tech. Note*, October, 1968.

[24] A. Palmgren, *Ball and Roller Bearing Engineering, 3rd ed*. Burbank, Philadelphia, PA, 1959.

[25] T. A. Harris and M. N. Kotzalas, *Advanced Concepts of Bearing Technology—Rolling Bearing Analysis*., CRC Press., Boca Raton, FL, 2007.

[26] P. H. Mellor, D. Roberts, and D. R. Turner, "Lumped parameter thermal model for electrical machines of TEFC design," *IEE Proc. B Electr. Power Appl.*, vol. 138, no. 5, p. 205, 1991

VIII. BIOGRAPHIES

Jun-Woo Chin received a Bachelor's degree in mechanical engineering from Hanyang University, Seoul, Korea, in 2014. He is currently working toward a Ph.D. in automotive engineering from Hanyang University.

His research interests are the design of electric machines and thermal analysis of electric motor and generator.

Sung-Woo Hwang received a Bachelor's degree in mechanical engineering from Hanyang University, Seoul, Korea, in 2014. He is currently working toward a Ph.D. in automotive engineering from Hanyang University.

His research interests are electric machine design for automotive and robot applications and numerical analysis of electromagnetics.

Hyeon-Jin Park received a Bachelor's degree in mechanical engineering from Hanyang University, Korea, in 2011. Currently he is pursuing Ph.D. degree in automotive engineering from Hanyang University, Korea.

His research interests are analysis, design, and optimization of electric machine and analysis of vibration caused by electro-magnetic force.

Jung-Pyo Hong (SM'97) received Ph.D. degree in electrical engineering from Hanyang University, Korea, in 1995. From 1996 to 2006, he was professor of Changwon National University, Chang-won, Korea. Since 2006 he has been working as a professor in the Hanyang University, Korea.

His research interests are the design of electric machines, optimization and numerical analysis of electromechanics.